A Pseudospectral Method for Time-Domain Computation of Electromagnetic Scattering by Bodies of Revolution

Baolin Yang and Jan S. Hesthaven

***Abstract*— We present a multidomain pseudospectral method for the accurate and efficient time-domain computation of scattering by body-of-revolution (BOR) perfectly electrically conducting objects. In the BOR formulation of the Maxwell equations, the azimuthal dependence of the fields is accounted for analytically through a Fourier series. The numerical scheme in the (r, z) plane is developed in general curvilinear coordinates and the method of characteristics is applied for patching field values in the individual subdomains to obtain the global solution. A modified matched-layer method is used for terminating the computational domain and special attention is given to proper treatment of the coordinate singularity in the scattered field formulation and correct time-domain boundary conditions along edges. Numerical results for monochromatic plane wave scattering by smooth and nonsmooth axis-symmetric objects, including spheres, cone-spheres, and finite cylinders, is compared with results from the literature, illustrating the accuracy and computational efficiency associated with the use of properly constructed spectral methods. To emphasize the versatility of the presented framework, we compute plane wave scattering by a missile and find satisfactory agreement with method-of-moment (MoM) computations.**

***Index Terms*— Bistatic radar cross section, body-of-revolution scattering, pseudospectral multidomain methods, time-domain scattering.**

I. Introduction

With the development of new technologies such as ultra-short pulse radars comes an increased need for the accurate and efficient modeling of very broad-band signals illuminating electrically large scatters.

In the past, the method-of-moments (MoM) has been extremely successful in addressing the problem of monochromatic plane wave scattering by very general objects. However, this choice of method is less attractive for these new types of problems for several reasons, e.g., the inherent monochromatic nature of the MoM makes the computation of broad-band scattering a very expensive process. Moreover, regions of multiple scattering or electrically very large objects are known to cause severe ill-conditioning and extremely large linear systems, stretching the limits of modern computers.

The need for broad-band excitation suggests the use of time-domain methods in which plane wave and short pulse excitation in handled with equal ease. Indeed, the advent of finite-difference time-domain (FDTD) methods [1] was partly driven by the need to solve large scattering problems being illuminated by a time-dependent source. Moreover, the FDTD approach has proven very fruitful in enabling the modeling of problems of very significant geometric complexity, possibly involving complex materials.

Although alleviating the problems associated with broad-band excitation, the mainstream FDTD method is troubled by the need of 10–20 points per wavelength to accurately resolve the wave dynamics of the scattering problem—and any other wave problem. The same phenomenon exists in the MoM approach and is an inherent consequence of these methods being of low order, e.g., most FDTD schemes are only second-order accurate. The accurate modeling of electrically large objects thus becomes prohibitive and either the required accuracy or the maximum electric size is severely limited.

The quest for high-accuracy time-domain solution and the ability to handle electrically large problems points toward high-order finite-difference methods as the proper tool for solving scattering problems and intensive effort have recently been put into devising such schemes for the Maxwell equations, e.g., [2], [3], yielding superior accuracy at the expense of a somewhat more complicated computational framework.

In the present work, we follow this line of thinking and develop pseudospectral time-domain methods suitable for the numerical solution of the scattering problem. To maintain geometric flexibility essential for the solution of problems of a practical character, we continue the work initiated in [4], [5] and formulate a multidomain scheme for the accurate and efficient computation of scattering by bodies-of-revolution (BOR). The pseudospectral schemes can be thought of as a maximum order finite-difference schemes and as such takes the role of the royals among numerical schemes for the solution of partial differential equations. As we shall learn properly formulated pseudospectral schemes yield not only superior accuracy but does so in a very efficient manner as compared to traditional low-order FDTD schemes.

The remaining part of this paper is organized as follows. In Section II, we develop the appropriate theoretical framework for the solution of the body-of-revolution (BOR) scattering problem in the time domain, with special attention being given to the treatment of the coordinate singularity and the specification of the proper boundary conditions on the perfectly conducting scatter. Section III is devoted to a discussion

Manuscript received September 8, 1997; revised June 11, 1998. This work was supported by DARPA/AFOSR Grant F49620-96-1-0426, DOE Grant DE-FG02-95ER25239, and NSF Grant ASC-9504002.

The authors are with the Division of Applied Mathematics, Brown University, Providence, RI 02912 USA.

Publisher Item Identifier S 0018-926X(99)03046-X.

of the multidomain pseudospectral framework in which we shall solve the Maxwell equations. The complete numerical scheme is studied quantitatively as well as qualitatively in Section IV, where we present results for scattering by a variety of objects excited by plane monochromatic waves of axial as well as oblique incidence and the results are compared with results from the literature. Section V contains a few concluding remarks and directions for future research.

II. The BOR Formulation of the Maxwell Equations

Consider the vacuum Maxwell equations in cylindrical coordinates (r, ϕ, z)

$$\varepsilon \frac{\partial \mathbf{E}}{\partial t} = \nabla \times \mathbf{H} \tag{1}$$

$$\mu \frac{\partial \mathbf{H}}{\partial t} = -\nabla \times \mathbf{E} \tag{2}$$

where $\mathbf{E} = (E_r, E_\phi, E_z)^T$ and $\mathbf{H} = (H_r, H_\phi, H_z)^T$ signify the electric and magnetic field components while ε and μ refer to the vacuum permitivity and permeability, respectively, related to the vacuum speed of light $c = (\varepsilon\mu)^{-1/2}$.

To arrive at the BOR formulation of the Maxwell equations, the azimuthal field variation is accounted for analytically through a Fourier expansion as

$$\mathbf{E}(r,\phi,z) = \sum_{m=0}^{\infty} (\tilde{\mathbf{e}}_u(r,z)\cos m\phi + \tilde{\mathbf{e}}_v(r,z)\sin m\phi) \tag{3}$$

$$\mathbf{H}(r,\phi,z) = \sum_{m=0}^{\infty} (\tilde{\mathbf{h}}_u(r,z)\cos m\phi + \tilde{\mathbf{h}}_v(r,z)\sin m\phi) \tag{4}$$

where m is the mode number and $\tilde{\mathbf{e}}_u = (\tilde{e}_{r,u}, \tilde{e}_{\phi,u}, \tilde{e}_{z,u})^T$, $\tilde{\mathbf{e}}_v = (\tilde{e}_{r,v}, \tilde{e}_{\phi,v}, \tilde{e}_{z,v})^T$, and likewise for $\tilde{\mathbf{h}}_u$ and $\tilde{\mathbf{h}}_v$. Hence, the first subscript refers to the field component, while the second subscript refers to its azimuthal variation.

We recall that while the scatterer is assumed to possess an axis symmetry, this is certainly not the case for the incident and scattered fields and introducing (3) and (4) only supplied an efficient way to account for the azimuthal variation of each individual mode.

Substituting (3) and (4) into (1) and (2) and utilizing the orthogonality of the trigonometric polynomials results in a pair of equations for the twelve unknowns, $\tilde{\mathbf{e}}_{u,v}$ and $\tilde{\mathbf{h}}_{u,v}$, for each azimuthal mode m as

$$\varepsilon \frac{\partial \tilde{\mathbf{e}}_{u,v}}{\partial t} = \nabla \times \tilde{\mathbf{h}}_{u,v} \pm \frac{m}{r}\hat{\boldsymbol{\phi}} \times \tilde{\mathbf{h}}_{v,u} \tag{5}$$

$$\mu \frac{\partial \tilde{\mathbf{h}}_{u,v}}{\partial t} = -\nabla \times \tilde{\mathbf{e}}_{u,v} \mp \frac{m}{r}\hat{\boldsymbol{\phi}} \times \tilde{\mathbf{e}}_{v,u}. \tag{6}$$

These twelve equations separate into two independent sets of equations in six unknowns, representing fields that are azimuthally orthogonal.

In various special cases, depending on angle of incidence and polarization of the incident wave, only one of the two sets of equations are needed to solve the problem. However, in the general case, we need to advance all twelve equations subject to an incident field on the form

$$\begin{Bmatrix} \mathbf{E}^{\text{inc}} \\ \mathbf{H}^{\text{inc}} \end{Bmatrix} = \begin{Bmatrix} \mathbf{E}^{i} \\ \mathbf{H}^{i} \end{Bmatrix} \exp[ik^i(\hat{\mathbf{k}}^i \cdot \mathbf{r} - ct)] \tag{7}$$

where $k^i = 2\pi/\lambda$ relates to the wavelength λ of the incident wave approaching the scatter along the propagation vector

$$\hat{\mathbf{k}}^i = -(\sin\theta^i \cos\phi^i \hat{\mathbf{x}} + \sin\theta^i \sin\phi^i \hat{\mathbf{y}} + \cos\theta^i \hat{\mathbf{z}})$$

where (θ^i, ϕ^i) specifies the direction of the incoming field in the usual spherical basis $(\hat{\boldsymbol{\rho}}, \hat{\boldsymbol{\theta}}, \hat{\boldsymbol{\phi}})$ and corresponding coordinates (ρ, θ, ϕ) with the exception that we have chosen to measure θ^i as the angle to $-\hat{\mathbf{z}}$ such that $\hat{\mathbf{k}} = \hat{\mathbf{z}}$ for axial incidence, i.e., $\theta^i = 0$. Unless otherwise stated, we shall only consider the case of $\phi^i = 0$ for simplicity.

The polarization of the incoming field is specified through the components along $\hat{\boldsymbol{\theta}}$ and $\hat{\boldsymbol{\phi}}$ as

$$\mathbf{E}^{\text{inc}} = E_\theta^{\text{inc}}\hat{\boldsymbol{\theta}} + E_\phi^{\text{inc}}\hat{\boldsymbol{\phi}}, \quad \mathbf{H}^{\text{inc}} = Z^{-1}\hat{\mathbf{k}}^i \times \mathbf{E}^{\text{inc}}$$

where $Z = \sqrt{\mu/\varepsilon} = 120\pi\Omega$ represents the intrinsic impedance. In accordance with standard notation, we refer to the case of $E_\phi^{\text{inc}} = 0$ as horizontally polarized while $E_\theta^{\text{inc}} = 0$ is termed vertically polarized excitation.

A. Treatment of the Axial Singularity

The BOR equations (5) and (6) contain a coordinate singularity at $r = 0$ that requires proper treatment. For the case of the total field formulation, a popular approach [1] is to use l'Hospitals rule at the axis to turn the singular terms into derivatives. However, when using the scattered field formulation, it remains unknown whether this limit exists and we must seek an alternative approach.

We apply a change of variables as

$$\mathbf{e}_{u,v} = r\tilde{\mathbf{e}}_{u,v}, \quad \mathbf{h}_{u,v} = r\tilde{\mathbf{h}}_{u,v}$$

which, after being introduced in (5) and (6), yields

$$\varepsilon \frac{\partial \mathbf{e}_{u,v}}{\partial t} = \nabla_\perp \times \mathbf{h}_{u,v} + \frac{1}{r}[(\mathbf{h}_{u,v} \cdot \hat{\mathbf{z}})\hat{\boldsymbol{\phi}} \pm m\hat{\boldsymbol{\phi}} \times \mathbf{h}_{v,u}] \tag{8}$$

$$\mu \frac{\partial \mathbf{h}_{u,v}}{\partial t} = -\nabla_\perp \times \mathbf{e}_{u,v} - \frac{1}{r}[(\mathbf{e}_{u,v} \cdot \hat{\mathbf{z}})\hat{\boldsymbol{\phi}} \pm m\hat{\boldsymbol{\phi}} \times \mathbf{e}_{v,u}] \tag{9}$$

where we have introduced $\nabla_\perp$ as the usual perpendicular vector operator in the (r, z) plane, i.e.,

$$\nabla_\perp = \hat{\mathbf{r}}\frac{\partial}{\partial r} + \hat{\mathbf{z}}\frac{\partial}{\partial z}.$$

Equations (8) and (9) still contains a number of singular terms at the axis. We shall consider the two cases of $m = 0$ and $m > 0$ separately.

$\underline{m = 0}$: In this case, we only have singularities in the equations of e_ϕ and h_ϕ. However, for $m \neq 1$, $\tilde{e}_\phi$ and $\tilde{h}_\phi$ are identically zero due to the nature of the fields at the axis [1] and we need not discretize the equations for the azimuthal field components at the axis but may simply impose the boundary conditions. Since these arguments are valid only for the total fields the boundary conditions for the scattered field are recovered by using the prescribed incident field.

$\underline{m > 0}$: This case is slightly more complicated in that we have singularities in all equations. However, for $m > 0$, the $\tilde{e}_z$ and $\tilde{h}_z$ components of the total fields are

identically zero along the axis since any constant-r Faraday's Law path integral containing $r = 0$ integrates to zero, i.e., e_z and h_z are both identically zero along the axis [1]. Rather than solving the equations for the axial components we simply impose the appropriate boundary condition which then couple into the equations of the radial variation. As for the case of $m = 0$, we must recover the scattered field boundary conditions using the incident fields for the remaining terms in (8) and (9) as the above argument is valid only for the total fields.

We note that the boundary conditions are arrived at without using approximations but rather derived solely on the basis of the properties of the fields and the knowledge of the prescribed incident fields along the axis.

B. Boundary Conditions at the Scatterer

To complete the specification of the problem, we need to address the question of boundary conditions at the scatterer.

Since we confine our attention to the case of perfectly electrically conducting (PEC) objects, the boundary conditions takes the general form

$$\bar{\mathbf{n}} \times \mathbf{E} = 0, \quad \bar{\mathbf{n}} \cdot \mathbf{H} = 0$$

where $\bar{\mathbf{n}} = (\bar{n}_r, \bar{n}_\phi, \bar{n}_z)$ represents an outward pointing unit-vector at the object.

For the sake of simplicity we shall deal with the azimuthal components seperately and introduce the (r, z) plane outward pointing normal vector $\hat{\mathbf{n}} = (\hat{n}_r, 0, \hat{n}_z)$.

Let us introduce the scattered field formulation as

$$\mathbf{E} = \mathbf{E}^{\text{inc}} + \mathbf{E}^s, \quad \mathbf{H} = \mathbf{H}^{\text{inc}} + \mathbf{H}^s$$

where the incident fields, $\mathbf{E}^{\text{inc}}$ and $\mathbf{H}^{\text{inc}}$, are prescribed at all times through (7). Considering the electric field we obtain, due to the symmetry, the condition

$$E_\phi^s = -E_\phi^{\text{inc}} \tag{10}$$

while a second condition is obtained by requesting

$$\hat{\boldsymbol{\phi}} \cdot (\hat{\mathbf{n}} \times \mathbf{E}^{\text{inc}}) = -\hat{\boldsymbol{\phi}} \cdot (\hat{\mathbf{n}} \times \mathbf{E}^s) = \hat{n}_r E_z^s - \hat{n}_z E_r^s. \tag{11}$$

This only yields one equation for the two unknown scattered field components. However, a third condition is arrived at by recalling the behavior of hyperbolic problems at solid walls, at which the outgoing characteristics are simply reflected [6]. Hence, for consistency we must also require that

$$\hat{\mathbf{n}} \cdot \mathbf{E}^s = \hat{n}_r E_r^s + \hat{n}_z E_z^s = \hat{\mathbf{n}} \cdot \mathbf{E}^{s,c} \tag{12}$$

where $\mathbf{E}^{s,c}$ signifies the computed scattered field. This yields the additional equation required to enforce the boundary condition on the electric field.

The situation for the magnetic field is very similar. Indeed, the physical condition yields

$$\hat{\mathbf{n}} \cdot \mathbf{H}^{\text{inc}} = -\hat{\mathbf{n}} \cdot \mathbf{H}^s = -\hat{n}_r H_r^s - \hat{n}_z H_z^s \tag{13}$$

while an additional condition appears as

$$\hat{\boldsymbol{\phi}} \cdot (\hat{\mathbf{n}} \times \mathbf{H}^s) = \hat{n}_z H_r^s - \hat{n}_r H_z^s = \hat{\boldsymbol{\phi}} \cdot (\hat{\mathbf{n}} \times \mathbf{H}^{s,c}) \tag{14}$$

where $\mathbf{H}^{s,c}$ refers to the computed scattered field.

While (10)–(14) uniquely determine the boundary conditions for the scattered field along smooth parts of the scatter, the formulation of boundary conditions along edges remains open.

The possibility of singular behavior of the field components along edges is detailed in [7] from which we infer that only E_ϕ and H_ϕ can be expected to be finite in the general case. If we term the angle $\alpha \in [0, 2\pi]$ of the wedge terminating in the edge, the remaining field components can be expected to scale as

$$E_r, E_z, H_r, H_z \sim t^{-(\pi-\alpha)/(2\pi-\alpha)}$$

where t signifies the distance to the edge. Hence, for convex wedges, $\alpha \in [0, \pi]$ the field components exhibit a weak singularity while all field components remain regular for concave wedges.

We can certainly not hope to resolve such singular behavior. However, boundary conditions are still required along the edges of convex wedges and we impose that E_ϕ vanishes at the edge while the remaining individual field components are continuous across the edge. While this is physically correct only for H_ϕ it is a reasonable assumption also for the remaining field components, which are still allowed to grow unboundedly in accordance with [7]. Moreover, the procedure ensures smooth fields for edges of concave wedges in accordance with the expected behavior.

III. The Numerical Scheme

In the following, we shall describe in some detail the individual elements of and the reasoning behind the complete multidomain scheme for the solution of (8) and (9) subject to the prescribed initial and boundary conditions.

A. Chebyshev Spectral Methods

The schemes presented in this paper are all based on Chebyshev collocation methods, which, due to their superior approximation properties, are widely used for the solution of partial differential equations.

The Chebyshev polynomial of order k is defined as

$$T_k(x) = \cos(k \cos^{-1} x)$$

where $|x| \leq 1$. In the following sections we will consider collocation methods, where the $N + 1$ collocation points are chosen to be the Chebyshev–Gauss–Lobatto points found as the roots of the polynomial $(1 - x^2)T_N'(x)$, i.e.,

$$x_i = -\cos\left(\frac{i\pi}{N}\right), \quad 0 \leq i \leq N.$$

When applying a Chebyshev collocation method, the function $f(x)$ is approximated by a grid function $f_i = f(x_i)$, where the grid points are the Gauss–Lobatto points. We construct a global Nth order Chebyshev interpolant I_N to obtain the approximation of the function

$$(I_N f)(x) = \sum_{i=0}^{N} f_i g_i(x).$$

The interpolating Chebyshev–Lagrange polynomials are given as

$$g_i(x) = \frac{(1-x^2)T_N'(x)(-1)^{i+1}}{c_i N^2 (x - x_i)}$$

where $c_0 = c_N = 2$ and $c_i = 1$ for $1 \leq i \leq N-1$. To seek approximate solutions $(I_N f)(x)$ to a partial differential equation, we ask that the equation is satisfied in a collocation sense, i.e., at the collocation points. Hence, we need to obtain values of the spatial derivatives at the collocation points. This is accomplished by approximating the continuous differential operator by a matrix operator with the entries

$$D_{ij} = g_j'(x_i)$$

such that the derivative of f at a collocation point x_i is approximated as

$$\frac{df}{dx}(x_i) \approx \frac{d(I_N f)}{dx}(x_i) = \sum_{j=0}^{N} D_{ij} f(x_j)$$

and, likewise, for higher derivatives. For the explicit expressions of the entries of the matrix operator and further details on collocation methods, we refer to [8].

The extension of this one-dimensional (1-D) framework to a multidimensional setting is most easily accomplished through the use of tensor products, e.g., given the function $f(x,y)$ we construct the two-dimensional approximation

$$(I_{M,N} f)(x,y) = \sum_{i=0}^{M} \sum_{j=0}^{N} f(x_i, y_j) g_i(x) g_j(y)$$

where we have introduced the Chebyshev Gauss–Lobatto grid y_j along y. The advantage of this approach is that derivatives are still computed through the use of 1-D differentiation matrices and matrix–matrix products. However, the use of tensor products also requires that $f(x,y)$ is defined on a rectangular grid, a restriction that we shall overcome shortly by introducing a multidomain formulation.

Filtering of the solution may be used when unresolved gradients are presents, as we may expect to be the case at edges. In the implementation of the present scheme, we employ an exponential filter of the type

$$\sigma_i = \begin{cases} 1 & 0 \leq i \leq N_c \\ \exp\left[-\alpha\left(\dfrac{i - N_c}{N - N_c}\right)^{\gamma}\right] & N_c < i \leq N \end{cases} \tag{15}$$

where N_c is a cutoff mode number, γ is the order of the filter, and $\alpha = -\ln \varepsilon_M$, with ε_M being the machine accuracy. This choice of filter function is by no means unique and alternatives may be found in [8]. The filtering may conveniently be expressed as a matrix operator F with the entries

$$F_{ij} = \frac{2}{c_j N} \sum_{k=0}^{N} \frac{\sigma_k}{c_k} T_k(x_i) T_k(x_j).$$

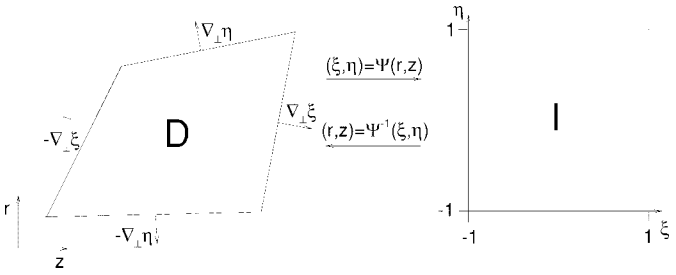

Fig. 1. Illustration of the mapping between physical coordinates, (r,z) and general curvilinear coordinates (ξ,η) required for the construction of the general multidomain scheme.

B. The (r,z) Equations in Curvilinear Form

The first step toward a geometrically flexible spectral scheme is to extend the use of polynomial expansions to the general curvilinear quadrilateral domain. We assume the existence of a smooth nonsingular mapping function Ψ relating the (r,z) coordinate system to the general curvilinear coordinate system (ξ,η) as

$$\xi = \xi(r,z), \quad \eta = \eta(r,z)$$

as illustrated in Fig. 1. We shall return to the actual specification and construction of the smooth map, Ψ, shortly.

Utilizing this notation transforms (8) and (9) into two hyperbolic systems

$$\frac{\partial \mathbf{q}_1}{\partial t} = A(\nabla_\perp \xi)\frac{\partial \mathbf{q}_1}{\partial \xi} + A(\nabla_\perp \eta)\frac{\partial \mathbf{q}_1}{\partial \eta} + \frac{1}{r}(C+D)\mathbf{q}_1 \tag{16}$$

and

$$\frac{\partial \mathbf{q}_2}{\partial t} = A(\nabla_\perp \xi)\frac{\partial \mathbf{q}_2}{\partial \xi} + A(\nabla_\perp \eta)\frac{\partial \mathbf{q}_2}{\partial \eta} + \frac{1}{r}(C-D)\mathbf{q}_2 \tag{17}$$

where we have the two state vectors

$$\mathbf{q}_1 = [e_{r,u}, e_{\phi,v}, e_{z,u}, h_{r,v}, h_{\phi,u}, h_{z,v}]^T$$
$$\mathbf{q}_2 = [e_{r,v}, e_{\phi,u}, e_{z,v}, h_{r,u}, h_{\phi,v}, h_{z,u}]^T$$

containing the twelve unknown field components. The form of (16) and (17) emphasizes that the two sets of equations differ only through the forcing term, constructed from the two matrices

$$C = \begin{bmatrix} 0 & 0 & 0 & 0 & 0 & 0 \\ 0 & 0 & 0 & 0 & 0 & 1/\varepsilon \\ 0 & 0 & 0 & 0 & 0 & 0 \\ 0 & 0 & 0 & 0 & 0 & 0 \\ 0 & 0 & -1/\mu & 0 & 0 & 0 \\ 0 & 0 & 0 & 0 & 0 & 0 \end{bmatrix}$$

and

$$D = \begin{bmatrix} 0 & 0 & 0 & 0 & 0 & m/\varepsilon \\ 0 & 0 & 0 & 0 & 0 & 0 \\ 0 & 0 & 0 & -m/\varepsilon & 0 & 0 \\ 0 & 0 & m/\mu & 0 & 0 & 0 \\ 0 & 0 & 0 & 0 & 0 & 0 \\ -m/\mu & 0 & 0 & 0 & 0 & 0 \end{bmatrix}.$$

The general operator $A(\mathbf{n})$ with $\mathbf{n} = (n_r, n_z)$ representing the local metric, is given as

$$\begin{bmatrix} 0 & 0 & 0 & 0 & -n_z/\varepsilon & 0 \\ 0 & 0 & 0 & n_z/\varepsilon & 0 & -n_r/\varepsilon \\ 0 & 0 & 0 & 0 & n_r/\varepsilon & 0 \\ 0 & n_z/\mu & 0 & 0 & 0 & 0 \\ -n_z/\mu & 0 & n_r/\mu & 0 & 0 & 0 \\ 0 & -n_r/\mu & 0 & 0 & 0 & 0 \end{bmatrix}.$$

This operator diagonalizes under the similarity transform $A(\mathbf{n}) = S^{-1}(\mathbf{n})\Lambda(\mathbf{n})S(\mathbf{n})$ where the diagonal eigenvalue matrix $\Lambda(\mathbf{n})$ has the entries

$$\Lambda(\mathbf{n}) = |\mathbf{n}| \operatorname{diag}[0, 0, c, c, -c, -c] \tag{18}$$

corresponding to two nonpropagating waves and two waves propagating along $\mathbf{n}$ with the speed of light, c, while two waves propagate along $-\mathbf{n}$ at the same speed. Here we have that $|\mathbf{n}|$ represents the length of the vector $\mathbf{n}$ such that $\mathbf{n} = |\mathbf{n}|(\hat{n}_r, \hat{n}_z)$. The diagonalizing matrix $S(\mathbf{n})$ is given as

$$S(\mathbf{n}) = \begin{bmatrix} \hat{n}_r & 0 & Z\hat{n}_z & 0 & -Z\hat{n}_z & 0 \\ 0 & 0 & 0 & Z & 0 & Z \\ \hat{n}_z & 0 & -Z\hat{n}_r & 0 & Z\hat{n}_r & 0 \\ 0 & \hat{n}_r & 0 & -\hat{n}_z & 0 & \hat{n}_z \\ 0 & 0 & 1 & 0 & 1 & 0 \\ 0 & \hat{n}_z & 0 & \hat{n}_r & 0 & -\hat{n}_r \end{bmatrix}$$

from which we may obtain

$$\mathbf{R} = S^{-1}(\mathbf{n})\mathbf{q} = \begin{bmatrix} R_1 \\ R_2 \\ R_3 \\ R_4 \\ R_5 \\ R_6 \end{bmatrix} = \frac{1}{2}\begin{bmatrix} 2\mathbf{e}\cdot\tilde{\mathbf{n}} \\ 2\mathbf{h}\cdot\tilde{\mathbf{n}} \\ (\mathbf{h} + Z^{-1}\tilde{\mathbf{n}}\times\mathbf{e})\cdot\hat{\phi} \\ (Z^{-1}\mathbf{e} - \tilde{\mathbf{n}}\times\mathbf{h})\cdot\hat{\phi} \\ (\mathbf{h} - Z^{-1}\tilde{\mathbf{n}}\times\mathbf{e})\cdot\hat{\phi} \\ (Z^{-1}\mathbf{e} + \tilde{\mathbf{n}}\times\mathbf{h})\cdot\hat{\phi} \end{bmatrix}$$

which we recognize as the characteristic variables, propagating along $\mathbf{n}$, with the speeds given by the entries of $\Lambda(\mathbf{n})$ (18). Here we have used the general form $\mathbf{q} = [\mathbf{e}, \mathbf{h}]^T$ and introduced $\tilde{\mathbf{n}} = (n_r, 0, n_z)$ for clarity.

Besides from revealing information about the dynamics of the fields, the identification and use of characteristic variables plays (as we shall see shortly) an integral role in the specification of the multidomain scheme.

C. The Multidomain Formulation

We wish to solve (16) and (17) within a general computational domain $\Omega \in \mathsf{R}^2$ in the (r, z) plane with $r \geq 0$. As we have briefly discussed, the most natural and computational efficient way of applying polynomial expansions in several dimensions is through the use of tensor products. This procedure, however, requires that the computational domain can be smoothly mapped to the unit square. To surround this quite severe limitation, we construct Ω using K nonoverlapping general curvilinear quadrilaterals, $\mathsf{D}^k \subset \mathsf{R}^2$ such that $\Omega = \bigcup_{k=1}^{K} \mathsf{D}^k$.

The advantages of such an approach, besides from providing the geometric flexibility, are many. In connection with spectral methods, the multidomain framework results in a lower total operation count and increased allowable time-step while providing a very natural data-decomposition, well suited for the implementation on contemporary parallel computers. We refer to [9] and [10] for a thorough discussion of the advantages associated with a multidomain formulation when solving wave-dominated problems.

Once we have split the global computational domain into K subdomains, we need to construct the map $\Psi : \mathsf{D} \to \mathsf{I}$, (see Fig. 1) where $\mathsf{I} \subset \mathsf{R}^2$ is the unit square, i.e., $\mathsf{I} \in [-1, 1]^2$. At this point, we have the Cartesian coordinates $(r, z) \in \mathsf{D}$ and the general curvilinear coordinates $(\xi, \eta) \in \mathsf{I}$ related through the map $(x, y) = \Psi(\xi, \eta)$. To establish a one-to-one correspondence between the unit square and the general quadrilateral we construct the local map for each subdomain using transfinite blending functions [11]. We refer to [12] for a thorough account of this procedure within the present context.

Once the global map Ψ has been constructed, we may compute the metric of the mapping and outward pointing normal vectors at all points of the enclosing edges of the quadrilateral.

Within the multidomain setting we need to solve K independent problems in the individual subdomains. However, to obtain the global solution we must pass information between the subdomains in a way consistent with the dynamics of the Maxwell equations. Since (16) and (17) constitute a hyperbolic system, it is natural to transfer information between the various subdomains using the characteristic variables $\mathbf{R}$, which are convected along the normal $\hat{\mathbf{n}}$ with a speed given by the diagonal elements of $\Lambda(\mathbf{n})$ (18). Hence, once the outward normal vector at the enclosing boundary of the subdomain is known we may uniquely determine which characteristics are leaving the subdomain and which are entering and, thus, need specification. We observe from (18) that while R_3 and R_4 are always leaving the domain and, therefore, need no boundary conditions, R_5 and R_6 are always entering the computational domain and require specification to ensure wellposedness. Based on this observation, we sketch in Fig. 2 the scheme for patching of two subdomains D^1 and D^2 sharing the common edge Γ. The two characteristic variables R_3^1 and R_4^1 leaving D^1 supply the sought-after boundary conditions for R_5^2 and R_6^2 and, reversely, for the specification of R_5^1 and R_6^1. For the nonpropagating R_1 and R_2, we use the average across Γ. Once the characteristic variables have been adjusted, the physical fields are recovered through the relation $S(\mathbf{n})\mathbf{R} = \mathbf{q}$. This procedure is applied along all interface points, including the vertices where it is done dimension-by-dimension, to arrive at the global solution at each times-step. As we shall see shortly, this procedure of patching hyperbolic systems is stable as well as accurate. Moreover, in a parallel setting the communication between subdomains grows only like the surface of the geometric building block rather than the volume.

D. Far-Field Boundary Conditions

A long-standing problem in computational electromagnetics is the issue of finding infinite space solutions on a finite computational domain. The central problem is how to construct appropriate boundary conditions that prevent outgoing waves from being reflected from the artificial numerical boundaries.

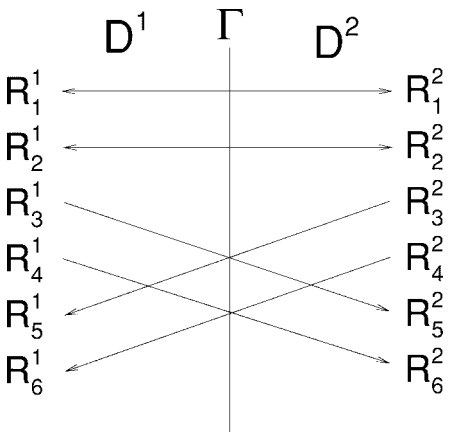

Fig. 2. Illustration of the patching of subdomains through the use of characteristic variables.

Characteristic boundary condition is used in different numerical schemes in many types of applications (see, e.g., [13]). It can serve as an absorbing boundary condition by imposing the incoming characteristic variables to be zero. However, it was shown in [4] that the accuracy of the approach is limited, in particular when the artificial boundary is placed close to the scatterer.

The introduction of the perfectly matched layer (PML) methods [14] has spawned significant research into such methods. Moreover, the development of well-behaved PML methods suitable for the BOR formulation of the Maxwell equations remains an open challenge.

In [4], we introduced a matched layer (ML) method, well suited for use in connection with multidomain methods, although not perfectly matched. An absorbing layer introduced through terms like $-\sigma(\xi,\eta)\mathbf{q}_{1,2}$ in (16) and (17), is put in the outermost subdomain at some distance from the subdomain interface and a cubic grid mapping is used to generate a mesh that is coarse in the part of the outer subdomain covered by the layer. With the help of a low-pass filter, the reflections in the ML region (being of high frequency relative to the local grid) is then being filtered out. Despite its simplicity, the ML method was shown to perform very well in [4], with the additional advantage of being simple to implement.

IV. Numerical Experiments

To validate the accuracy and computational efficiency of the complete computational framework discussed in the previous sections, we have computed plane wave scattering by a number of perfectly conducting bodies of revolution, previously studied through the use of analytic methods or alternative numerical schemes, e.g., BOR MoM [15].

To assess the accuracy of the computational framework we use the bistatic radar cross section (RCS) $\sigma(\theta,\phi)$ representing a measure between the time-averaged incident and scattered fields as [16]

$$\sigma(\theta,\phi)=\lim_{r\to\infty}4\pi r^2\frac{|\mathbf{E}^s_\infty|^2}{|\mathbf{E}^{\mathrm{inc}}|^2}$$

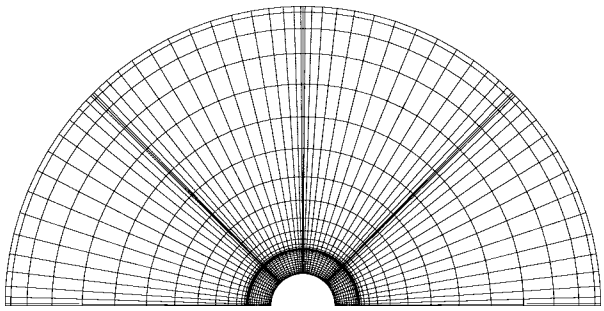

Fig. 3. Typical multidomain grid for the computation of scattering by a sphere. Note the stretching of the grid in the outer subdomains in order to successfully absorb outgoing waves in the ML layer without increasing the computational work.

where (θ,ϕ) measures the angles between the incident wave vector $\mathbf{k}^i$ and the scattered wave vector $\mathbf{k}^s$, given as

$$\mathbf{k}^s=Z\frac{\mathbf{E}^s_\infty\times\mathbf{H}^s_\infty}{|\mathbf{E}^s_\infty|^2}$$

where $\mathbf{E}^s_\infty$ and $\mathbf{H}^s_\infty$ signifies the far-field values of the scattered fields. Unless otherwise stated, we normalize σ with the square of the wavelength λ of the incident wave and define

$$\mathrm{RCS}(\theta,\phi)=10\log_{10}\frac{\sigma(\theta,\phi)}{\lambda^2}.$$

As we are only computing the near fields, we apply a near-field to far-field transformation [1] with the enclosing surface being chosen to coincide with grid lines. A Chebyshev–Clenshaw–Curtis integration [8] is used for approximating the integrals.

Only the scattered fields are computed and the objects are illuminated through the boundaries as discussed in Section II-B. To advance the fields in time, we use a fourth-order Runge–Kutta scheme [8] and we enforce the boundary conditions as well as perform the patching of the local solutions at the intermediate time-steps of the integration. The time-step is chosen below the stability limit to avoid severe dispersion errors and we apply a filter, as described in Section III-A, with $N_c=0$ and $\gamma\sim N$ following the completion of each time-step.

A. Scattering by a Sphere

Scattering by perfectly conducting spheres serves as an optimal test case since the analytical solution is known through a Mie series [17]. We need only consider axial illumination, i.e., only the $m=1$ mode in (3) and (4) is required due to the symmetry of the scatterer and the properties of the fields. In accordance with standard notation, the RCS is normalized with πa^2 rather than with the wavelength of the incident wave.

In Fig. 3, we show a typical grid layout for the computation of scattering by the sphere. We use eight subdomains in two layers surrounding the upper half $(r\geq 0)$ of the sphere with the number of modes in each subdomain depending on the electrical size of the problem.

In Fig. 4, we compare the analytic solution for plane wave scattering by a $ka=8.3$ sphere with the solution obtained using the multidomain scheme with $K=8$ as in Fig. 3

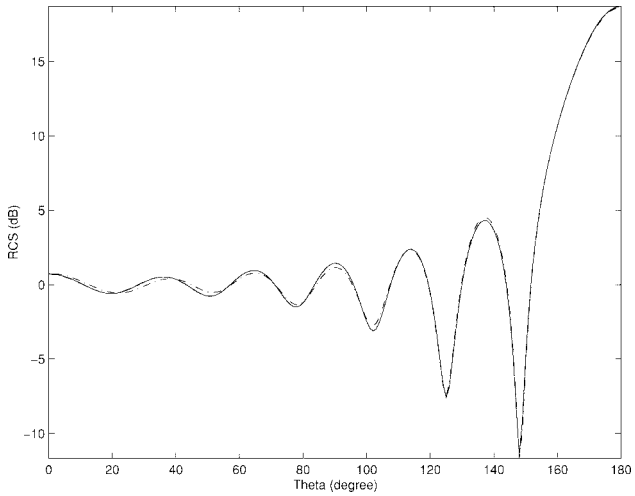

Fig. 4. $\mathrm{RCS}(\theta, 0)$ for a perfectly conducting sphere $ka = 8.3$. We compare the exact Mie series (dashed), the spectral multidomain solution with characteristicboundary conditions (dashed-dotted), and using theML far-field boundary conditions (full).

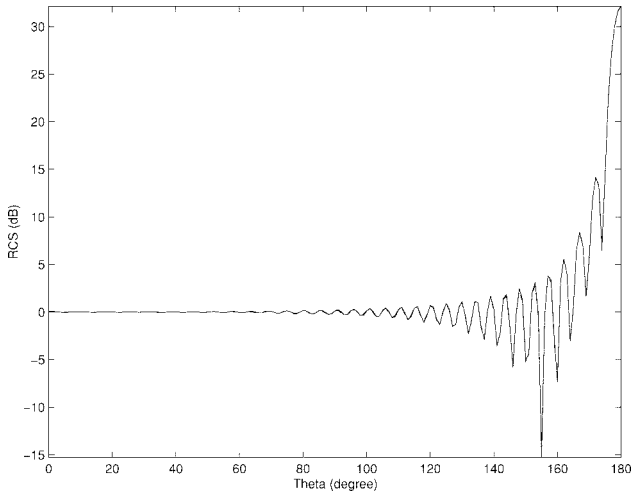

Fig. 5. $\mathrm{RCS}(\theta, 0)$ for a perfectly conducting sphere $ka = 40.0$. We compare the exact Mie series (dashed) and the spectral multidomain solution using the ML far-field boundary conditions (full).

and $N = 16$ in all domains. For the numerical solution, we use either characteristic boundary conditions or the ML layer technique discussed in Section III-D. Indeed, we clearly observe the second-order accuracy of the characteristic boundary conditions [4] in the back scatter region while the ML solutions and the analytic solution overlap completely, illustrating the expected accuracy of the spectral multidomain framework.

To emphasize the strength of spectral methods when addressing electrically large problems, we show in Fig. 5 a comparison between the analytic solution and the computed solution obtained with a $K = 20$ and $N = 16$ spectral multidomain solution for a $ka = 40.0$ sphere. Indeed, we find (even in the highly sensitive backscatter region) close to perfect agreement between the two solutions. The solution shown in Fig. 5 is obtained in about 20 min using an average-sized work station.

Although scattering from a sphere may serve as an excellent starting point for the evaluation of a new numerical scheme, it is certainly of only marginal practical importance. In the following, we shall study the performance of the multidomain scheme for scattering problems of a more general character. Due to lack of analytic solutions we shall compare the computed RCS with results taken from the open literature.

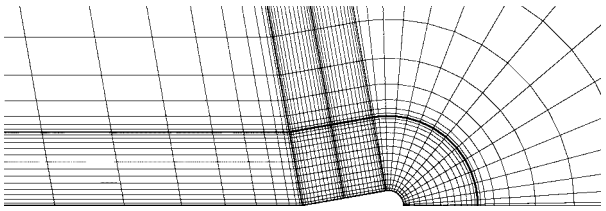

Fig. 6. Fraction of a typical multidomain grid for the computation of plane wave scattering by a smooth sphere cone.

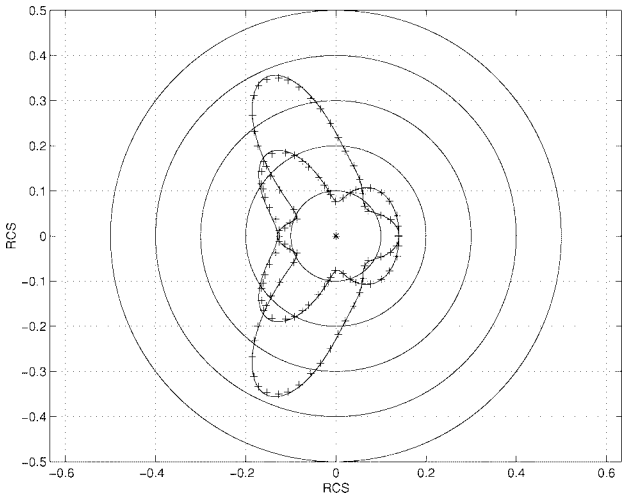

Fig. 7. $\mathrm{RCS}(\theta, 0)$ for smooth cone sphere with axial incidence. The reference solution, marked by "+," is taken from [15].

B. Scattering by Generic Objects—Axial Incidence

Due to the simplicity of the problem, i.e., we only need to consider the $m = 1$ mode in (3) and (4), let us first look at scattering of plane waves impinging axially.

In Fig. 6, we show part of a typical grid for the computation of scattering by a 20° cone smoothly joined with a spherical cap having a radius of 0.2λ. This case was first considered in [15] in which the problem is solved using a MoM scheme.

The RCS, as computed using $K = 8$ and $N = 16$ in all domains, is compared in Fig. 7 with the results reported in [15] for horizontal and vertical polarization of the incident fields. As this is an electrically small object, we should expect excellent agreement between the MoM result [15] and the multidomain solution as is observed in Fig. 7.

A more challenging test is that of plane wave scattering by a 45° cone joined nonsmoothly with a spherical cap of radius $kr = 10$. The length of the scatter is $ka = 20$, similar to the problem considered in [18]. We recall that the field components in the (r, z) plane may exhibit weak singular behavior as discussed in Section II-B.

In Fig. 8, we compare the computed RCS for axial incidence with the results reported in [18]. Indeed, compared with the

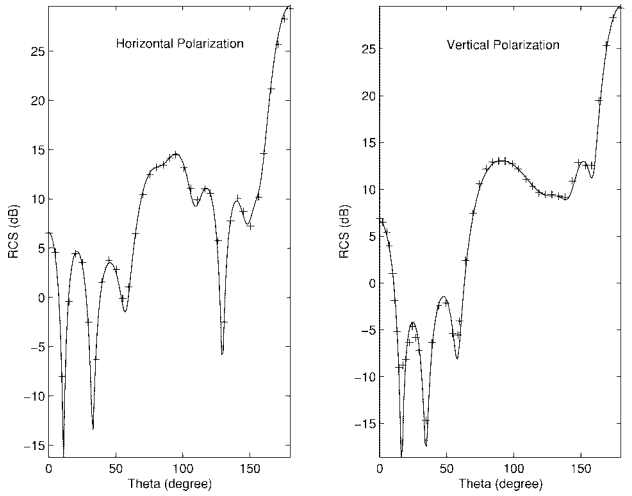

Fig. 8. $\mathrm{RCS}(\theta, 0)$ for nonsmooth cone sphere with axial incidence. The reference solution, marked by "+," is taken from [18].

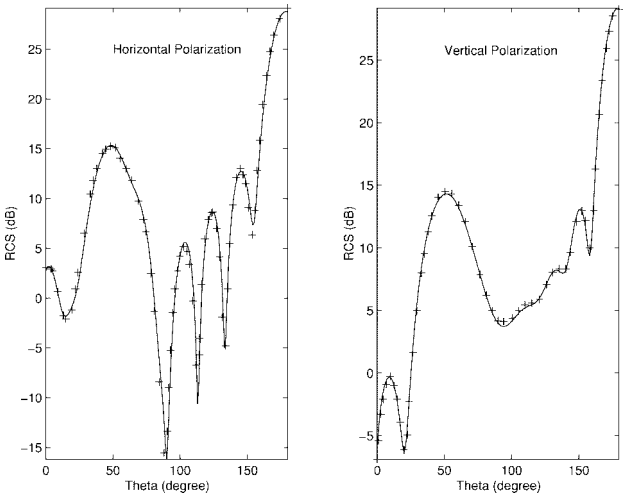

Fig. 10. $\mathrm{RCS}(\theta, 0)$ for scattering of a 20° obliquely incident wave by a nonsmooth cone sphere. The reference solution, marked by "+," is taken from [18].

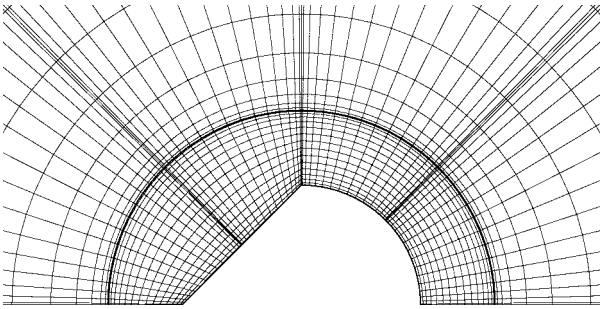

Fig. 9. Typical multidomain grid used for the computation of scattering by a nonsmooth sphere cone.

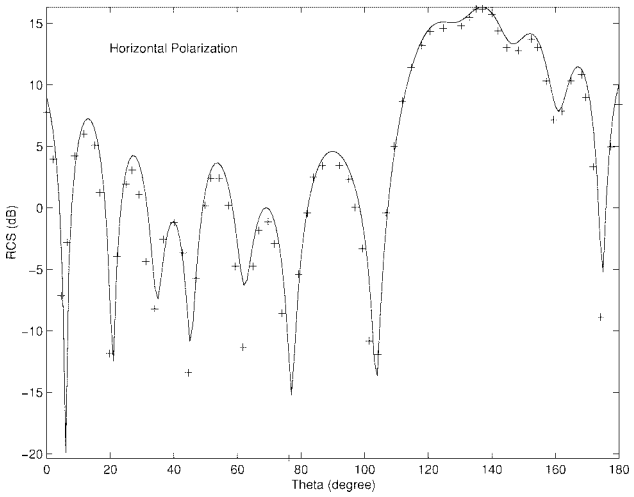

Fig. 11. $\mathrm{RCS}(\theta, 60)$ for scattering by a finite cylinder, illuminated by a horizontally polarized plane wave impinging at 45°. The reference solution, marked by "+," is taken from [19].

scenario in Fig. 7, we observe a dramatic increase in the dynamic range of the RCS due to the larger electric size and increased geometric complexity, but we maintain excellent agreement between the reference and the results obtained using the multidomain spectral scheme. The grid, a fraction of which is shown in Fig. 9, consists of $K = 8$ domains, each employing a resolution of $N = 16$ modes in each direction. We note, in particular, that no effort has been put into selective refinement of the grid around the edges, something that would have been crucial in case a low-order scheme was used.

C. Scattering by Generic Objects—Oblique Incidence

As the next level of added complexity, we consider scattering by generic objects much as in the previous sections, however, subject to oblique illumination. This problem is more complicated in that the number of modes required in the azimuthal expansions of the fields (3) and (4) is larger than for axial incidence.

The number of modes required in the azimuthal expansion is naturally problem dependent. However, since the fields can be assumed to possess a high degree of regularity one can expect that only a few modes will yield accurate results.

The first case, the grid of which is shown in Fig. 9, is the nonsmooth cone sphere considered in the last section, but illuminated with a wave impinging at 20°. We use 12 Fourier modes to approximate the azimuthal field variation. The grid is similar to the case of axial illumination and in Fig. 10 we compare the computed RCS with the solution reported in [18] and observe excellent agreement over a more than 40-dB dynamic range.

As a second example of oblique scattering we consider scattering by a finite cylinder, illuminated by a plane wave impinging at 45°. The length as well as the radius of the cylinder is 2λ and we use a $K = 12$ and $N = 16$ grid for solving the problem which was considered in [19].

In Fig. 11 we show the computed cross section, obtained using 14 Fourier modes that was found to be enough to arrive at a converged result and compare with the results of [19] for horizontal polarization. The result for vertical polarization is given in Fig. 12 and we observe close agreement between the different approaches to the scattering problem, confirming the accuracy, and efficacy of the spectral multidomain scheme.

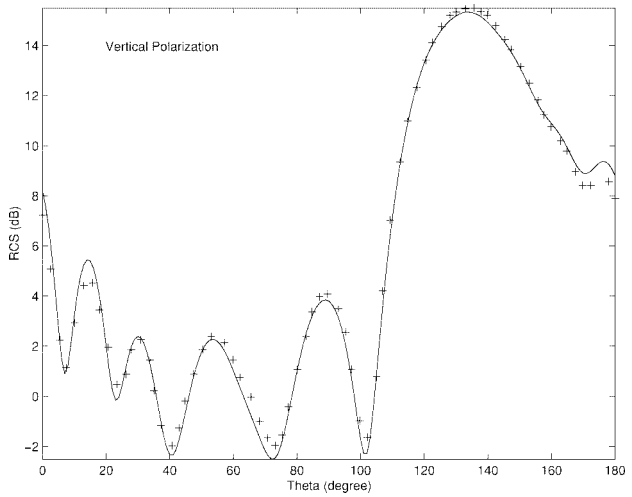

Fig. 12. $\mathrm{RCS}(\theta, 60)$ for scattering by a finite cylinder, illuminated by a vertically polarized plane wave impinging at 45°. The reference solution, marked by "+," is taken from [19].

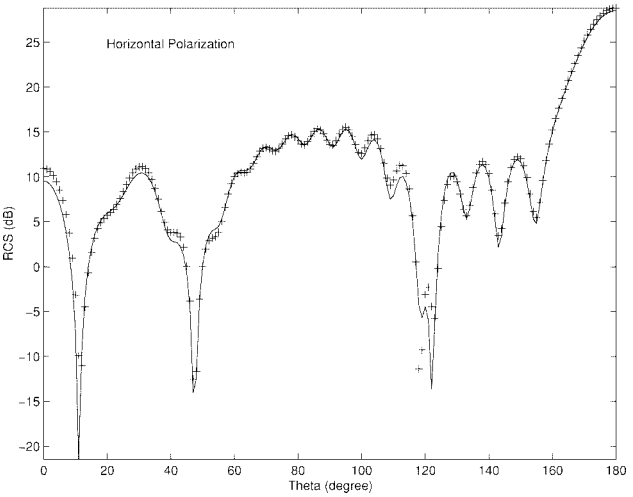

Fig. 14. $\mathrm{RCS}(\theta, 0)$ for a missile subject to axial illumination by a horizontally polarized plane wave. The reference solution, marked by "+," was provided by [20].

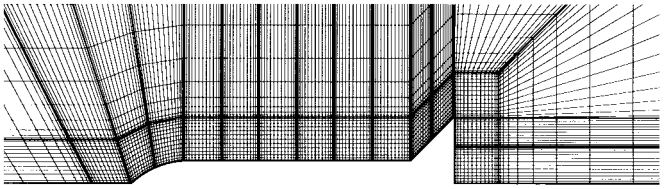

Fig. 13. Typical multidomain grid for the solution of the scattering by a missile.

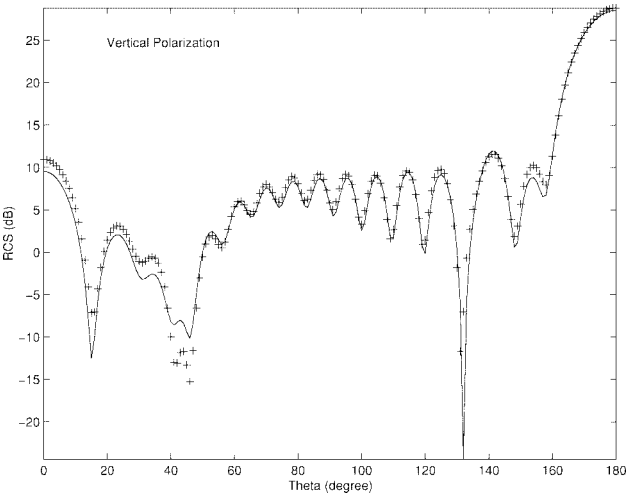

Fig. 15. $\mathrm{RCS}(\theta, 0)$ for a missile subject to axial illumination by a horizontally polarized plane wave. The reference solution, marked by "+," was provided by [20].

D. Scattering by General Objects

As a final illustration of the versatility of the multidomain scheme for the accurate modeling of scattering by objects of arbitrary geometric complexity, we consider the problem of scattering by a perfectly conducting missile illuminated by a 4-GHz plane wave at axial/nose incidence. The missile is about 7.25 wavelengths long and the diameter of the main body is one wavelength.

In Fig. 13 we show a fraction of the computational grid, illustrating that while the object is of only moderate electric size, it is of considerable geometric complexity and contains features like a sharp wedge at the tail. The grid is constructed using $K = 31$ subdomains, each employing a resolution of $N = 16$.

For axial incidence of a horizontally polarized plane wave, in Fig. 14 we show the computed cross section compared with that obtained using a standard MoM approach [20]. We observe excellent agreement to within a few decibels over a dynamic range of close to 60 dB. The difference between the present solution and the MoM solution is most pronounced in the backscatter region, which is well known to be very sensitive to modeling errors. In Fig. 15 we compare the results for the case of vertical polarization.

V. Concluding Remarks

The purpose of this paper has been twofold. We wanted, on one hand, to illustrate to the reader the benefits of using high-order/spectral multidomain schemes for the solution of problems in electromagnetics—in this case, the scattering problem. As we have shown through numerous examples, the use of pseudospectral multidomain methods for the time-domain solution of scattering problems yields not only results of superior accuracy, but does so in a very efficient manner compared with more conventional low-order FDTD schemes. Indeed, computational electromagnetics of the future will require long time integration of problems involving electrically large structures—a scenario for which the use of high-order/pseudospectral methods is likely to be the optimal choice of method.

The second objective of this paper was to continue the development and evaluation of the pseudospectral time-domain method initiated in our previous work [4], [5] in which we dealt with two-dimensional problems. Here, we have developed a multidomain scheme for the computation of scattering by arbitrary bodies of revolution and illustrated

the superior properties of such a scheme through numerous computations and comparisons with results from the literature.

Although the development of the BOR scheme opens up for the computation of large complex axis-symmetric bodies, hitherto intractable through direct numerical modeling, many issues remain open in the quest toward a general purpose multidomain pseudospectral scheme. Apart from issues like grid generation (a severe problem independent of the method of choice) we need to address problems beyond the pure scattering problem discussed here. Indeed, the development and evaluation of high-order/pseudospectral schemes for problems involving various types of materials remains the most immediate open issue and we hope to report on developments along these lines in the near future.

ACKNOWLEDGMENT

The authors would like to thank Prof. D. Gottlieb, Brown University, for many inspiring conversations. They would also like to thank Dr. J. S. Shang, WPAFB, who provided them with several test cases and general encouragement, and Dr. T. B. Hansen, ERCS/Rome Lab, and Prof. O. Breinbjerg, Technical University of Denmark, who both helped illuminate the intricacies of edges.

REFERENCES

[1] A. Taflove, *Computational Electrodynamics—The Finite-Difference Time-Domain Method*. Boston, MA: Artech House, 1995.
[2] P. G. Petropoulous, "Phase error control for FDTD methods of second- and fourth-order accuracy," *IEEE Trans. Antennas Propagat.*, vol. 42, pp. 859–862, June 1994.
[3] B. Yang and D. Gottlieb, "Comparisons of staggered and nonstaggered schemes for Maxwell's equations," in *Proc. 12th Annu. Rev. Progress Appl. Computat. Electromagn.*, Naval Postgraduate School, Monterey, CA, Mar. 1996, vol. II, pp. 1122–1131.
[4] B. Yang, D. Gottlieb, and J. S. Hesthaven, "Spectral simulations of electromagnetic wave scattering," *J. Comput. Phys.*, vol. 134, no. 2, pp. 216–230, 1997.
[5] ———, "On the use of PML ABC's in spectral time-domain simulations of electromagnetic scattering," in *Proc. 13th Annu. Rev. Progress Appl. Computat. Electromagn.*, Naval Postgraduate School, Monterey, CA, Mar. 1997, vol. II, pp. 926–934.
[6] D. Gottlieb, M. Gunzburger, and E. Turkel, "On numerical boundary treatment for hyperbolic systems," *SIAM J. Numer. Anal.*, vol. 19, pp. 671–697, 1982.
[7] J. Meixner, "The behavior of electromagnetic fields at egdes," *IEEE Trans. Antennas Propagat.*, vol. AP-20, no. 4, pp. 442–446, July, 1972.
[8] C. Canuto, M. Y. Hussaini, A. Quarteroni, and T. A. Zang, *Spectral Methods in Fluid Dynamics—Springer Series in Computational Physics*. ——— New York: Springer-Verlag, 1987.
[9] P. Fischer and D. Gottlieb, "On the optimal number of subdomains for hyperbolic problems on parallel computers," *Int. J. Supercomputer Appl. High-Performance Comput.*, vol. 11, no. 1, pp. 65–76, 1997.
[10] J. S. Hesthaven, "A stable penalty method for the compressible Navier-Stokes equations. II. One dimensional domain decomposition schemes," *SIAM J. Sci. Comp.*, vol. 18, pp. 658–685, 1997.
[11] W. J. Gordon and C. A. Hall, "Transfinite element methods: Blending-function interpolation over arbitrary curved element domains," *Numer. Math.*, vol. 21, pp. 109–129, 1973.
[12] J. S. Hesthaven, "A stable penalty method for the compressible Navier-Stokes equations. III. Multi dimensional domain decomposition schemes," *SIAM J. Sci. Comp.*, to be published.
[13] J. S. Shang, "Time-domain electromagnetic scattering simulations on multicomputers," *J. Computat. Phys.*, vol. 128, no. 2, pp. 381–390, 1996.
[14] J. P. Berenger, "A perfectly matched layer for the absorption of electromagnetic waves," *J. Computat. Phys.*, vol. 114, pp. 185–200, 1994.
[15] J. R. Mautz and R. F. Harrington, "Radiation and scattering from bodies of revolution," *Appl. Sci. Res.*, vol. 20, pp. 405–435, 1969.
[16] E. F. Knott, J. F. Shaeffer, and M. T. Tuley, *Radar Cross Section*. Boston, MA: Artech House, 1993.
[17] J. J. Bowman, T. B. A. Senior, and P. L. E. Uslenghi, *Electromagnetic and Acoustic Scattering by Simple Shapes*. New York: Hemisphere, 1987.
[18] L. N. Medgyesi-Mitschang and D. Wang, "Hybrid solutions for scattering from perfectly conducting bodies of revolution," *IEEE Trans. Antennas Propagat.*, vol. AP-31, pp. 570–583, June 1983.
[19] S. D. Gedney and R. Mittra, "The use of the FFT for the efficient solution of the problem of electromagnetc scattering by a body of revolution," *IEEE Trans. Antennas Propagat.*, vol. 38, no. 3, pp. 313–322, 1990.
[20] J. S. Shang, private communication, 1997.

Baolin Yang received the B.S. degree from Nanjing University, Nanjing, China, and the M.S. degree from the Institute of Computational Mathematics and Scientific/Engineering Computing, Chinese Academy of Sciences, Beijing, China, in 1990 and 1993, respectively

He is currently a graduate student in the Division of Applied Mathematics, Brown University.

Mr. Yang won the President's Prize of the Chinese Academy of Sciences for excellent graduate student in 1993.

Jan S. Hesthaven received the M.Sc. and Ph.D. degrees, in applied mathematics/numerical analysis, from the Technical University of Denmark in 1991 and 1995, respectively.

He is currently an National Science Foundation (NSF) Postdoctoral Fellow and Visiting Assistant Professor in the Division of Applied Mathematics, Brown University.

His main interest is in the theory and application of high-order/spectral methods for the solution of problems in, e.g., electromagnetics, gas-dynamics, acoustics and nonlinear optics, with a current emphasis on multidomain methods for wave-dominated problems in general geometries.